Heliyon 10 (2024) e29587

Contents lists available at ScienceDirect

Heliyon

journal homepage: www.cell.com/heliyon

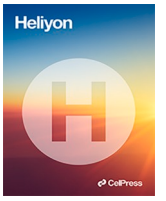

Research article

Integrated bioinformatics analysis and experimental animal models identify a robust biomarker and its correlation with the immune microenvironment in pulmonary arterial hypertension

Mukamengjiang Juaiti [a], Yilu Feng [a], Yiyang Tang [a], Benhui Liang [a], Lihuang Zha [a,b,**], Zaixin Yu [a,b,*]

[a] Department of Cardiology, Xiangya Hospital, Central South University, Changsha, Hunan, 410008, P.R. China
[b] National Clinical Research Center for Geriatric Disorders, Xiangya Hospital, Central South University, Changsha, Hunan, 410008, P.R. China

ARTICLE INFO

Keywords:
Pulmonary arterial hypertension
Robust biomarkers
Differential gene expression
Immune cell infiltration
BPIFA1

ABSTRACT

Background: Pulmonary arterial hypertension (PAH) represents a substantial global risk to human health. This study aims to identify diagnostic biomarkers for PAH and assess their association with the immune microenvironment through the utilization of sophisticated bioinformatics techniques.

Methods: Based on two microarray datasets, differentially expressed genes (DEGs) were detected, and hub genes underwent a sequence of machine learning analyses. After pathways associated with PAH were assessed by gene enrichment analysis, the identified genes were validated using external datasets and confirmed in a monocrotaline (MCT)-induced rat model. In addition, three algorithms were employed to estimate the proportions of various immune cell types, and the link between hub genes and immune cells was substantiated.

Results: Using SVM, LASSO, and WGCNA, we identified seven hub genes, including (BPIFA1, HBA2, HBB, LOC441081, PI15, S100A9, and WIF1), of which only BPIFA1 remained stable in the external datasets and was validated in an MCT-induced rat model. Furthermore, the results of the functional enrichment analysis established a link between PAH and both metabolism and the immune system. Correlation assessment showed that BPIFA1 expression in the MCP-counter algorithm was negatively associated with various immune cell types, positively correlated with macrophages in the ssGSEA algorithm, and correlated with M1 and M2 macrophages in the CIBERSORT algorithm.

Conclusion: BPIFA1 serves as a modulator of PAH, with the potential to impact the immune microenvironment and disease progression, possibly through its regulatory influence on both M1 and M2 macrophages.

* Corresponding author. Department of Cardiology and National Clinical Research Center for Geriatric Disorders, Xiangya Hospital, Central South University, Changsha, Hunan, P.R. China.

** Corresponding author. Department of Cardiology and National Clinical Research Center for Geriatric Disorders, Xiangya Hospital, Central South University, Changsha, Hunan, P.R. China.

E-mail addresses: zhalihuang@csu.edu.cn (L. Zha), yuzaixin@126.com (Z. Yu).

https://doi.org/10.1016/j.heliyon.2024.e29587
Received 17 March 2023; Received in revised form 9 April 2024; Accepted 10 April 2024
Available online 16 April 2024

1. Introduction

Pulmonary arterial hypertension (PAH) is a severe cardiovascular condition threatening the heart and lung functions [1]. The diagnostic process usually involves right heart catheterization to measure pulmonary artery pressure. The criteria include a pulmonary pressure exceeding 20 mmHg, a pulmonary artery wedge pressure of ≤15 mmHg, and pulmonary vascular resistance of ≥3 Woods units [2]. There are some approved medications for PAH, such as guanylate cyclase stimulators, phosphodiesterase inhibitors, prostacyclin analogs, receptor agonists, and endothelin receptor antagonists [3]. These drugs primarily expand the pulmonary artery vascular system and reduce pulmonary vascular resistance, providing relief from symptoms but not completely reversing vascular remodeling or significantly extending overall survival [4]. Despite treatment improvements, the 5-year survival rate continues to be relatively low, ranging from 57% to 59%, emphasizing the need for a more profound understanding of PAH pathogenesis and its associated biomarkers [5].

Pulmonary vascular remodeling is one of the significant pathological features of PAH involving excessive thickening of the vascular wall, which leads to narrowing or occlusion of the lumen [6]. Functional impairment predominantly impacts the intrinsic cells comprising endothelial cells, smooth muscle cells, and adventitial fibroblasts situated within the vascular wall [7]. Endothelial cells, located in the inner layer of blood vessels, play a crucial role in blood clotting prevention and regulation of vasodilation and vasoconstriction by releasing substances such as nitric oxide (NO) and prostacyclin (PGI2) [8]. Simultaneously, smooth muscle cells in the vessel middle layer possess the ability to contract and relax, influencing vessel diameter, and consequently, blood flow [9]. Adventitial fibroblasts, primarily found in the outer layer of vessels, are responsible for generating and maintaining connective tissues, including collagen and elastic fibers. These tissues are fundamental components in maintaining vascular structure and function [10]. Recent studies have shown that immune cells, specifically macrophages and lymphocytes, are crucial in the development of PAH [11–13]. Through the release of inflammatory and cytokine components, specifically tumor necrosis factor (TNF) and interleukin (IL), these immune cells impact the functioning of cells in the vascular wall, leading to a deterioration of pulmonary vascular remodeling [14]. The immune response in PAH depends on maintaining a delicate equilibrium between pro- and anti-inflammatory elements, and any disturbance to this balance can lead to vascular injury and remodeling [15]. Therefore, understanding these complex interactions in the immune microenvironment is crucial for providing substantial support for the treatment and prevention of PAH.

Recently, with rapid advancements in next-generation sequencing (NGS) techniques, new perspectives for tackling this issue are provided based on holistic strategies in systems biology [16]. A growing body of evidence indicates a connection between PAH and metabolism disruptions, with the participation of the immune system in the onset and advancement of PAH [11,17,18]. Despite these findings, the absence of widely applicable and sensitive biomarkers for clinical use leads to significant difficulties in clinical diagnosis and treatment, particularly in devising strategies for early detection and monitoring. Hence, revealing the molecular mechanisms that contribute to the development of PAH is imperative. To address these challenges, we used diverse bioinformatics analysis techniques to explore the differentially expressed genes (DEGs) between individuals with and without PAH, identify robust biomarkers, and investigate the relationship between the immune microenvironment and nutritional metabolism; in addition, we delineated distinct gene expression patterns and validated them using external gene datasets; finally, pivotal hub genes were selected and confirmed in an animal model of PAH. This all-encompassing methodology broadens our understanding and establishes the groundwork for the formulation of targeted therapeutic approaches.

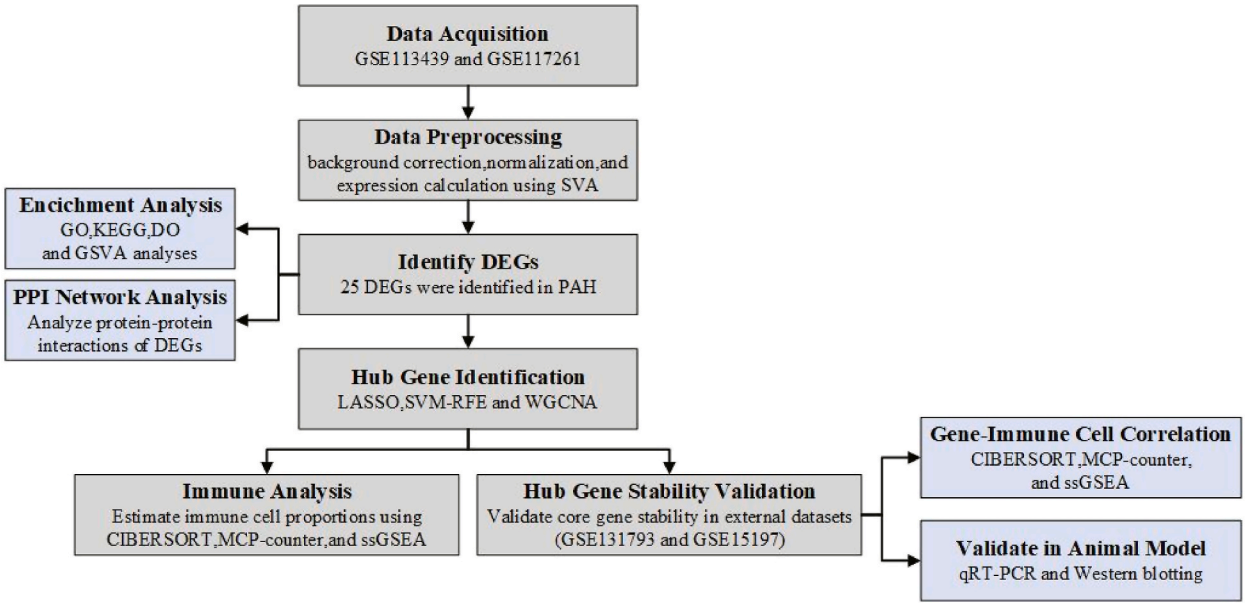

Fig. 1. Research workflow.

2. Materials and method

2.1. Datasets and data pre-processing

Fig. 1 shows a flowchart outlining our study. Two microarray datasets (GSE113439 and GSE117261) of pulmonary artery tissues were obtainedfrom the GEO database (https://www.ncbi.nlm.nih.gov/geo/). After background correction and normalization of raw data, we calculated gene expression patterns in PAH using the SVA program package [19]. Principal component analysis (PCA) was performed to eliminate batch effects (Supplementary Figure S1). External validation datasets (GSE131793 and GSE15197) were subjected to similar preprocessing steps to ensure comparability. Applying consistent preprocessing to both the primary and validation datasets ensured the robustness of the comparative analysis. GSE113439 includes lung samples from 15 PAH patients and 11 healthy controls obtained during lobectomy for lung cancer. The PAH group consisted of patients with idiopathic PAH (n = 6), connective tissue diseases (CTD, n = 4), congenital heart disease (CHD, n = 4), and chronic thromboembolic pulmonary hypertension (CTEPH, n = 1). Additionally, GSE117261 contains gene expression data from 58 PAH and 25 control lung tissues.

2.2. Screening and validation of hub markers

DEGs in PAH versus normal specimens were identified through the *limma* package [20], using thresholds of | log 2 fold change (FC) | > 1 and $p < 0.05$. Then, the gtsummary package in R was used to perform Logistic Regression analysis on these DEGs [21]. Subsequently, hub genes underwent additional screening by the Least Absolute Shrinkage and Selection Operator (LASSO, glmnet package) with 10-fold cross-validation [22]. In addition, support vector machine-recursive feature elimination (Support Vector Machine [SVM]-RFE) is a machine learning method that relies on SVM [23]. Based on DEGs, the optimal core genes were identified after deleting the feature vectors through support vector machines (e1071 and msvmRFE packages) [24]. In Weighted Gene Co-expression Network Analysis (WGCNA) [25], all identified DEGs were used as input, and the clustering of all samples was good. A shear of 50 was established to exclude any outlier samples. Soft threshold levels from 1 to 20 were examined to identify an optimal soft threshold of 7, which was instrumental in transforming the correlation matrix into an adjacency matrix and further into a topological overlap matrix (TOM) for hierarchical clustering via an average linkage method. Modules were categorized based on the TOM, ensuring that each module contained no fewer than 50 genes. The gene modules used in this study were defined at a cut height of 0.3. For each module, gene significance (GS) and module membership (MM) values were computed to facilitate scatter plots generation. Finally, the correlation between the modules and clinical traits was tested using Pearson's method.

2.3. Protein-protein interaction analysis

In our study, we utilized the Search Tool for the Retrieval of Interacting Genes (STRING) database (http://string-db.org/) as a resource to predict protein-protein interactions (PPI) [26]. The PPI network of DEGs was constructed with a minimum interaction score of 0.4 and visualized in Cytoscape software (version 3.7.2) [27].

2.4. GO enrichment analysis

Gene Ontology (GO) enrichment analysis is frequently employed in identifying functional annotations significantly enriched in a specific set of genes [28]. We conducted GO enrichment analysis on identified core genes by the ClusterProfiler package in R [29]. In order to identify critical pathways involving the core genes, a pathway enrichment analysis was conducted using the Kyoto Encyclopedia of Genes and Genomes (KEGG) [30]. Furthermore, Disease Ontology (DO) analysis was performed in order to examine prospective diseases that may be linked to the core genes that were identified [31]. The results of KEGG, DO and GO analyses were represented graphically using the GOplot software application [32]. Moreover, critical signaling pathways related to hub genes were detected using ClusterProfile and Gene Set Variation Analysis (GSVA) packages [33]. The MSigDB c7 Immunesigdb V7.4 Symbols GMT gene sets, genes and gene expression matrix were used for GSVA analysis to explore the immune regulating pathway that may be involved in the identified core genes [34].

2.5. Construction of hub gene regulatory network

Initially, the mirDIP database was employed to predict potential miRNAs downstream of targeted hub genes [35], with a threshold at a very high minimum score to discern the regulatory network. Subsequently, Transcriptional Regulatory Relationships Unravelled by Sentence-based Text-mining (TRRUST) database, encompassing 800 individual transcription factors (TFs), was used to establish an upstream regulatory network [36], with TF-core genes ($p < 0.05$) chosen for interactions. Finally, the NetworkAnalyst database (https://www.networkanalyst.ca/) was used to visualize the regulatory networks of hub genes.

2.6. Immune analysis algorithm

The proportions of various immune cell types were estimated by analyzing gene expression data using the CIBERSORT package [37]. The resulting output provides information on the presence of 22 different immune cells, which can be used to generate an immune cell component matrix for further analysis. Based on transcriptome data, the abundance of 8 immune cell types and 2 stromal

cell populations in heterogeneous tissues [38] was quantified using the MCP counter algorithm. Lastly, based on relevant gene sets, enrichment of the immune cell fraction and immune pathway activity fraction was performed by the ssGSEA algorithm through the GSVA package [33].

2.7. Animal study

Animal experiments adhered to the Guidelines for the Care and Use of Experimental Animals. All animal procedures were approved by the Experimental Animal Ethics Committee of Central South University (No. 2021SYDW0110). Prior to experimentation, a one-week acclimation period was provided for all animals under controlled conditions, including unrestricted access to food and water, a temperature of 22 ± 1 °C, and a humidity range of 45–55%. This acclimation period lasted for a total of 24 h. The animals were separated into the control and MCT groups. After weighing the animals in the MCT group, a drug injection of 60 mg/kg body weight was administered to induce pulmonary hypertension, following the same feeding protocol as the control group.

RT-qPCRanalysis

Total RNA was isolated from each specimen utilizing the TRIzol agent (Thermo Fisher Scientific, Carlsbad, CA, USA), adhering to the protocols provided by the manufacturer. For mRNA expression analysis, the QuantiTect Reverse Transcription Kit (QIAGEN, Hilden, Germany) along with the SYBR Green PCR Kit (Thermo Fisher Scientific) were used. The PCR was executed using β-actin mRNA as an endogenous reference, employing the 7900HT Fast Real-Time PCR System (Applied Biosystems, Foster City, CA, USA). Primer sequences applied were as follows:

BPIFA1:

Forward 5′-CCAGACACCCACTGAGACCT-3’.

Reverse 5′-TCCAAACCGCTGAGAATCCC-3’.

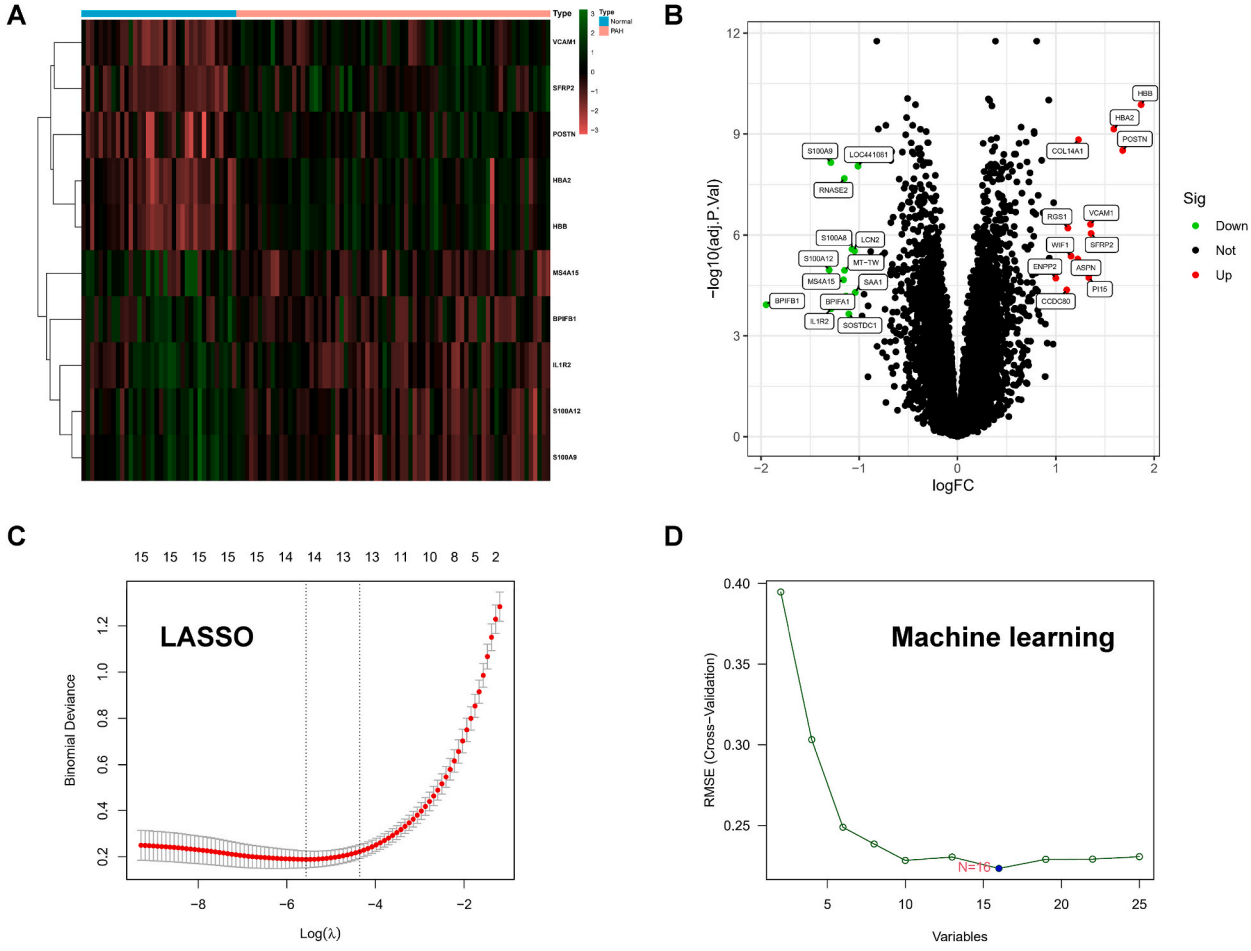

Fig. 2. Differentially expressed genes and hub biomarker screening.(A) The heatmap visualizes the top 10 differentially expressed genes (DEGs).(B) The volcano plot reveals 25 DEGs, with genes experiencing upregulation marked in red and those undergoing downregulation depicted in green.(C)LASSO regression analysis.(D)Machine learning method of SVM. (For interpretation of the references to colour in this figure legend, the reader is referred to the Web version of this article.)

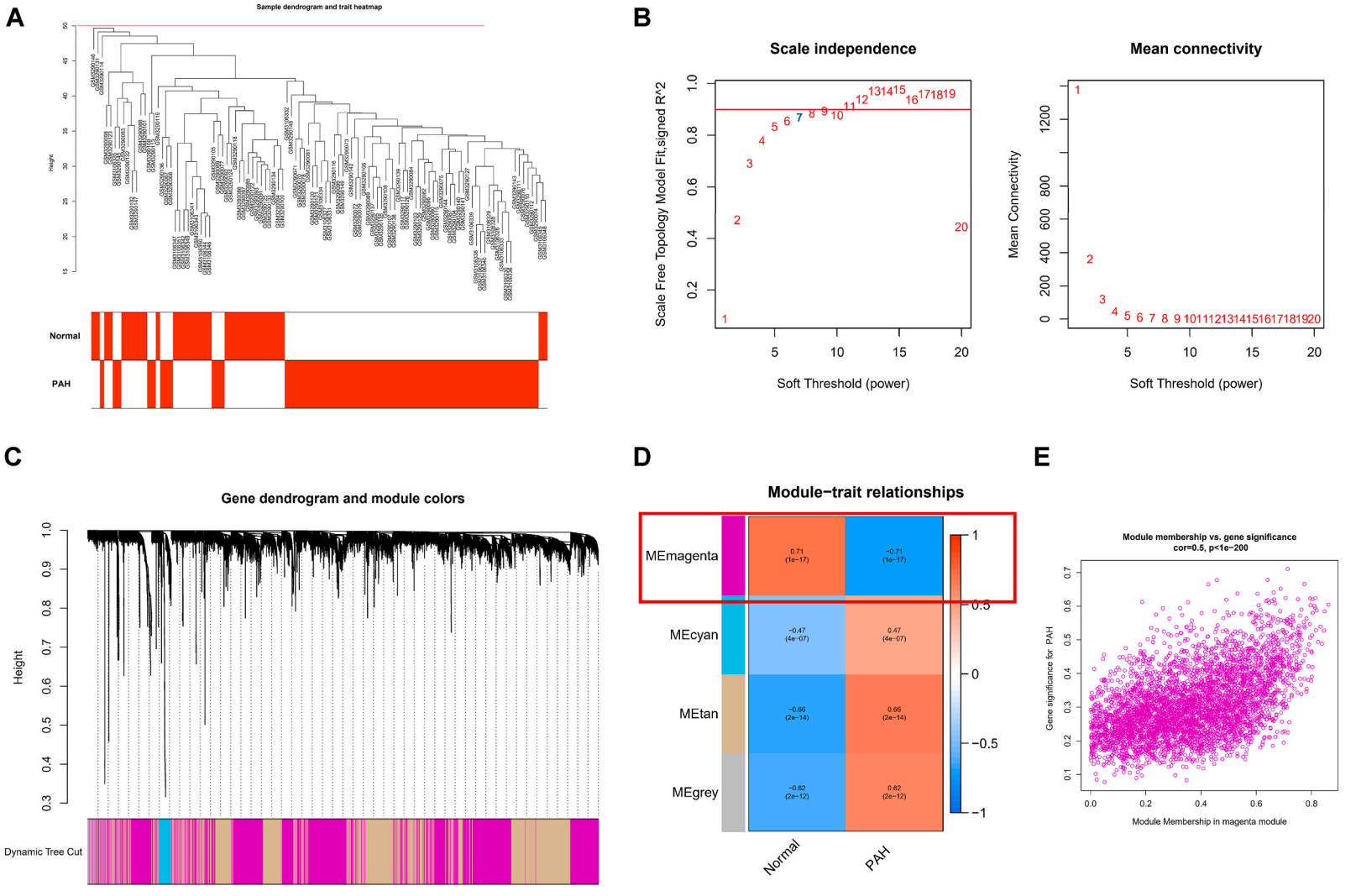

Fig. 3. WCGNA analysis.(A) The sample, excluding one outlier and employing a shear line threshold of 50, was deemed effective. (B) Topological calculations using soft thresholds ranging from 1 to 20 were performed to ascertain the optimal soft threshold of 7. (C) Utilizing soft thresholds, the relationship matrix was transformed into an adjacency matrix, which was further converted to a topological overlap matrix (TOM) for the purpose of average link hierarchy clustering, subsequently categorizing the relevant modules based on TOM. (D) An analysis of the correlation between genes within modules and clinical traits revealed that the green module exhibited the highest correlation with the incidence of PAH ($p = -0.71$). (E)The scatter plot delineates the correlation between gene significance (GS) and module membership (MM) for 4003 genes within the green module. (For interpretation of the references to colour in this figure legend, the reader is referred to the Web version of this article.)

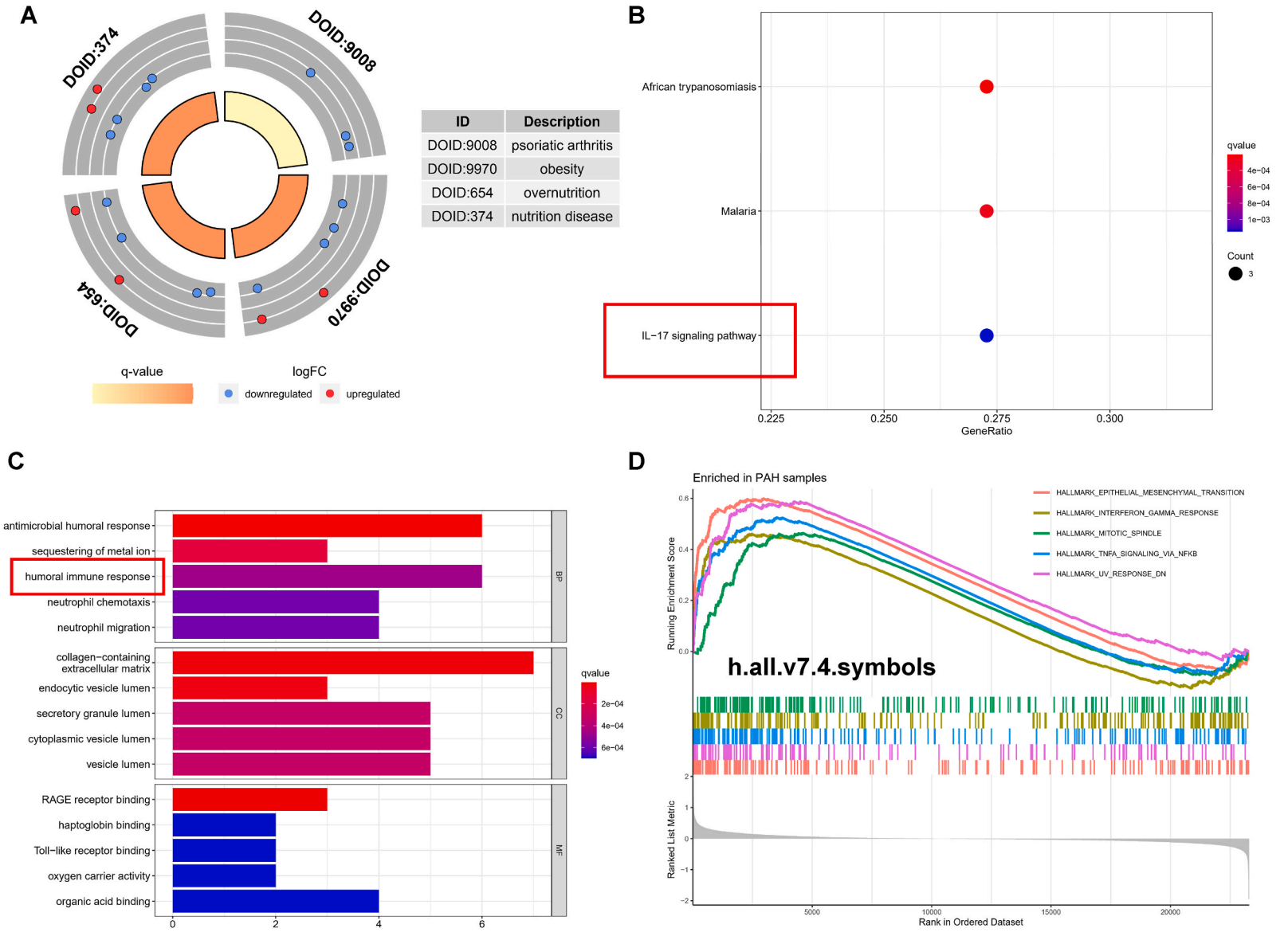

Fig. 4. Enrichment analysis. (A) DO analysis (B) KEGG analysis (C) GO enrichment analysis (D) GSVA analysis.

β-actin:
Forward 5′-CGT TGA CAT CCG TAA CGA CTCC-3′,
Reverse 5′-ATA GAGCCA CCA TTC CGA CAC AG-3’.
Western blotting (WB).

Lung tissues from rats were disrupted for protein isolation using the radioimmunoprecipitation assay (RIPA) buffer (PC101; EpiZyme, China). The concentration of the proteins was determined with a bicinchoninic acid (BCA) assay kit (ZJ101, China) obtained from EpiZyme. Following this, the protein extracts were subjected to SDS-PAGE, and subsequently, the separated proteins were transferred to a polyvinylidene fluoride (PVDF) membrane. This membrane was then blocked and incubated with primary antibodies against BPIFA1 (1:500, sc-398,376, Santa Cruz) at 4 °C overnight. For normalization, an Alpha Tubulin Polyclonal Antibody (1:500011224-1-AP, Protein) served as the internal standard. The membrane underwent four washes, each lasting 5 min, before being exposed to a secondary antibody (1:10,000, SA00001-2, and SA00001-1; Proteintech) at 37 °C for 40 min.

2.8. Statistical analysis

All statistical computations were conducted using R software (v.4.0.1). The antecedent section provides an exhaustive description of the statistical procedures utilized in the processing of transcriptome data. Statistical significance is established as $p < 0.05$.

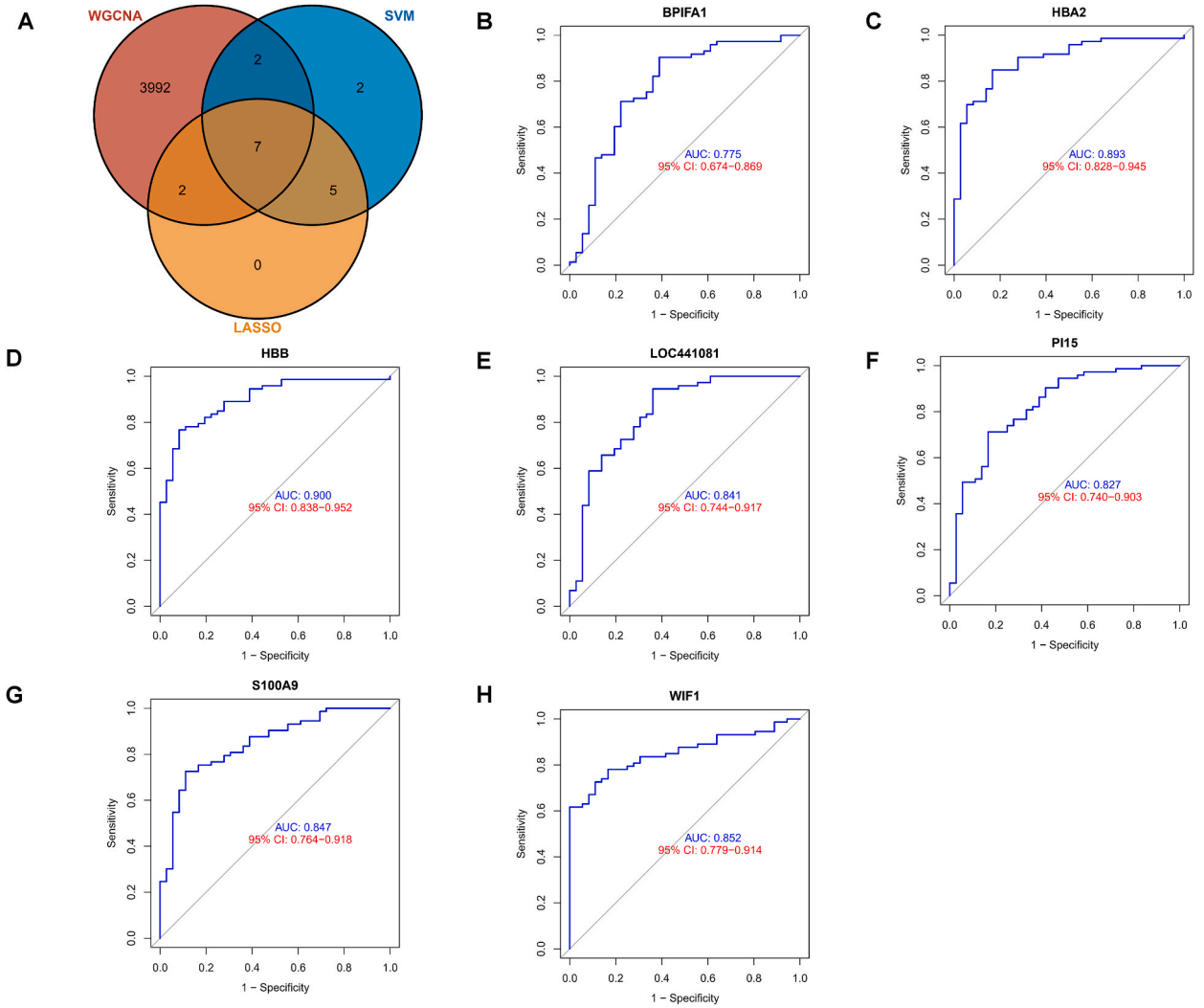

Fig. 5. Investigating the prognostic significance of biomarkers. (A) An integrated approach combining WGCNA, machine learning techniques and LASSO was employed to pinpoint potential candidate genes. (B–H) ROC analysis was conducted on the identified genes to evaluate their predictive accuracy.

3. Results

3.1. LASSO analysis and machine learning algorithm integration for hub biomarker screening

We used the GSE113439 and GSE117261 datasets to screen for DEGs using the 'limma' program package. 25 DEGs were identified in total and a heat map was generated to display the top ten DEGs ranked using logFC (Fig. 2A). A volcano plot indicated that 12 genes (HBB, HBA2, COL14A1, POSTN, VCAM1, RGS1, SFRP2, WIF1, ASPN, PI15, ENPP2, and CCDC80) were upregulated and 13 genes (S100A9, LOC441081, RNASE2, S100A8, LCN2, S100A12, MT-TW, MS4A15, SAA1, BPIFA1, BPIFB1, IL1R2, and SOSTDC1) were downregulated in PAH endothelial tissues (Fig. 2B). In addition, logistic regression analysis showed that these 25 DEGs remained stable, demonstrating consistent and significant differences (Figure S2A). Moreover, we constructed a PPI network for the DEGs, which revealed 105 interactions (Figure S2B). To further identify the core genes among the 25 DEGs, we performed 10-fold cross-validation using LASSO and selected 14 candidate genes (Fig. 2C). Furthermore, we used the machine learning method of SVM to conduct a more comprehensive analysis and determined that the highest accuracy was achieved when 16 genes were included (Fig. 2D).

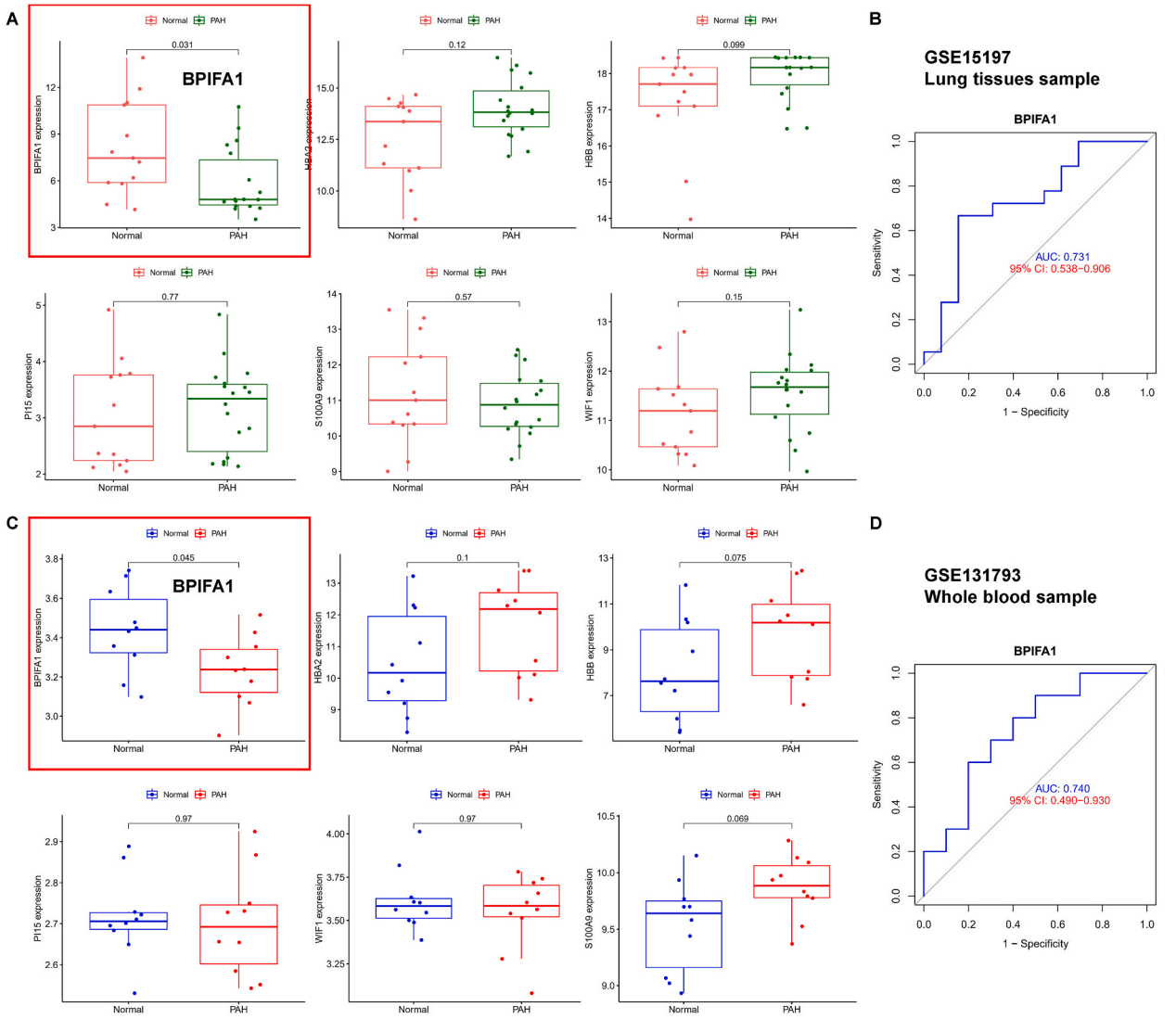

Fig. 6. Confirming the significance of hub biomarkers in external datasets: (A) Candidate genes were validated within the GSE15197 dataset, with those highlighted in red denoting stable expression. (B) The candidate gene BPIFA1 was subjected to ROC analysis within the GSE15197 dataset. (C) Validation of candidate genes was also conducted in the GSE131793 dataset, where genes marked in red signify stable expression levels. (D) The candidate gene BPIFA1 underwent a further ROC analysis within the GSE15197 dataset to ascertain its diagnostic performance. (For interpretation of the references to colour in this figure legend, the reader is referred to the Web version of this article.)

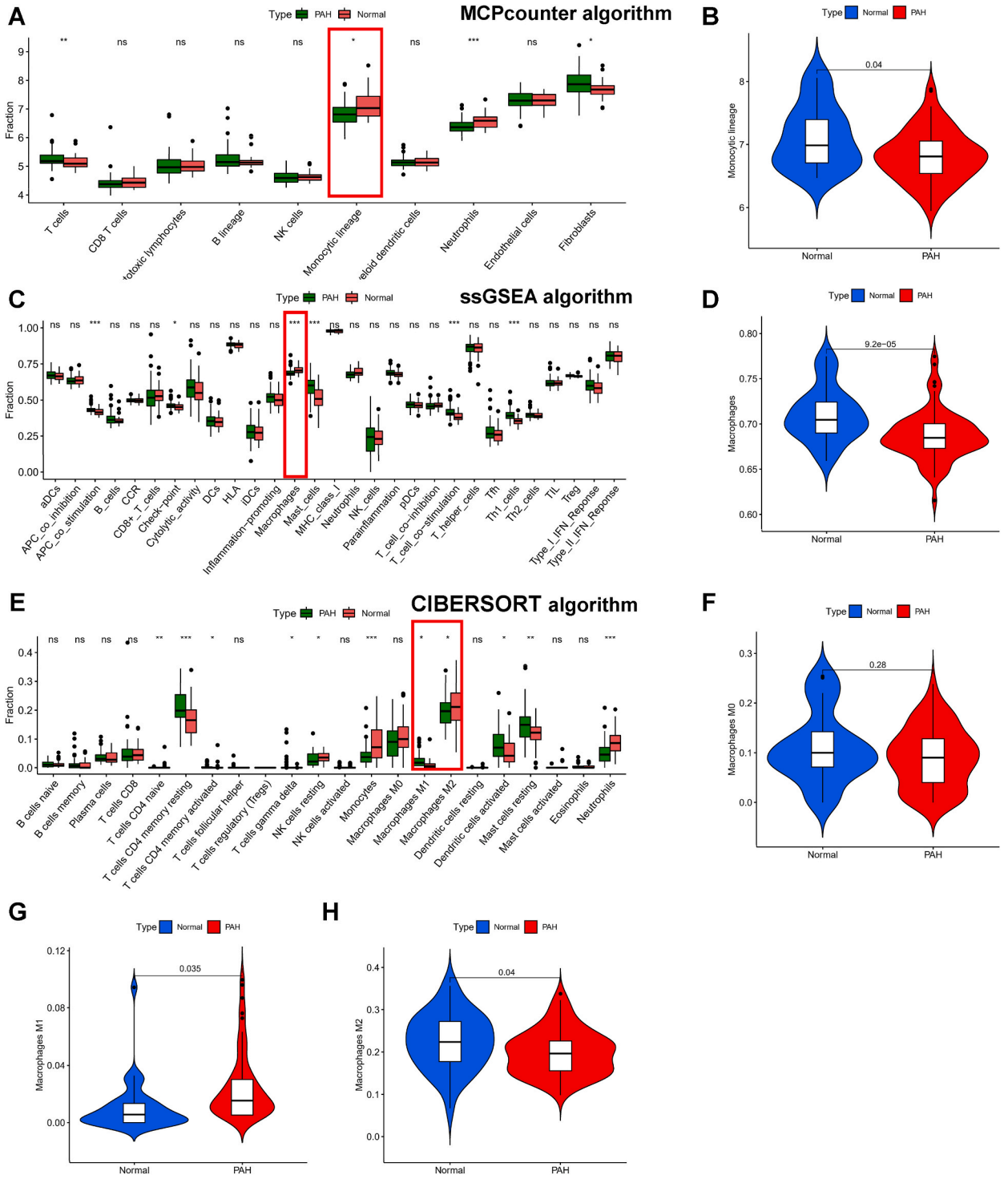

Fig. 7. Immune analysis. (A) Utilizing the MCP-counter algorithm, disparities in immune cell expression were identified. (B) Analysis of monocytic lineage across various tissues was conducted through the MCP-counter.(C)The ssGSEA algorithm facilitated a more precise categorization of immune cells. (D) Examination of monocytic lineage in diverse tissues was carried out using the ssGSEA. (E) Differential expression of immune cells was unveiled by the CIBERSORT algorithm. (F–H) The content of M0, M1, and M2 macrophage types was examined using the CIBERSORT algorithm. *p < 0.05, **p < 0.01, and ***p < 0.001.

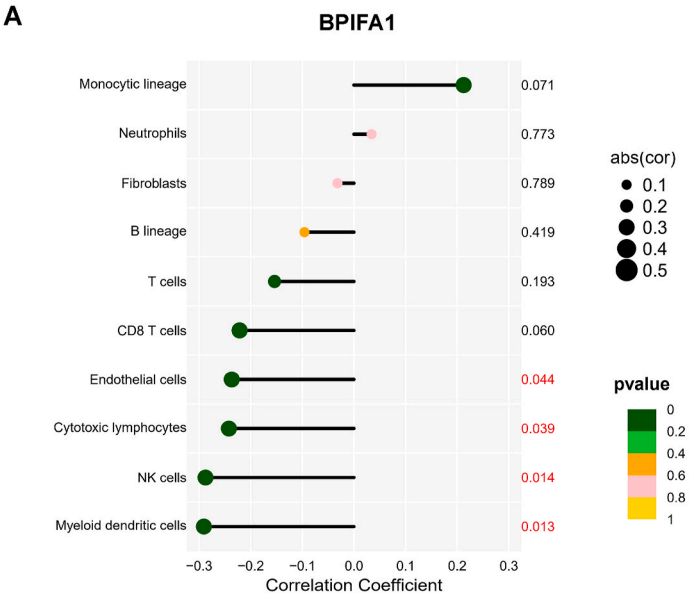
A
BPIFA1
Monocytic lineage 0.071
Neutrophils 0.773
Fibroblasts 0.789
B lineage 0.419
T cells 0.193
CD8 T cells 0.060
Endothelial cells 0.044
Cytotoxic lymphocytes 0.039
NK cells 0.014
Myeloid dendritic cells 0.013
−0.3 −0.2 −0.1 0.0 0.1 0.2 0.3
Correlation Coefficient
abs(cor)
0.1
0.2
0.3
0.4
0.5
pvalue
0
0.2
0.4
0.6
0.8
1

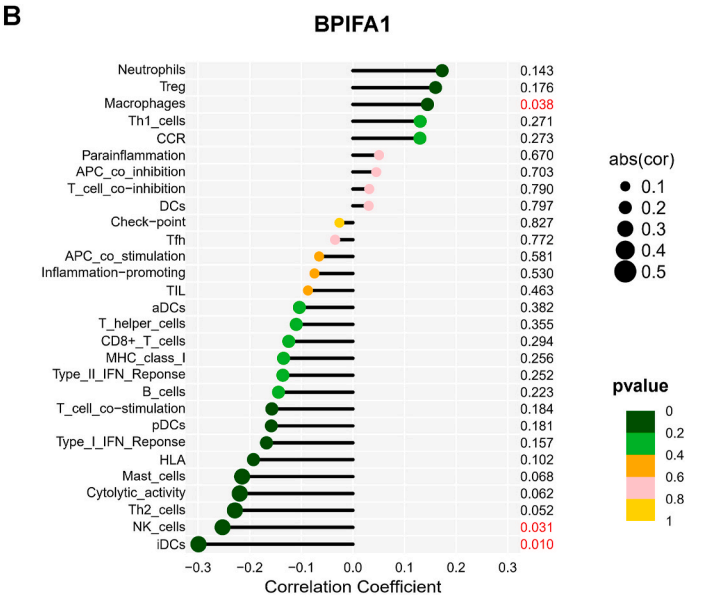
B
BPIFA1
Neutrophils 0.143
Treg 0.176
Macrophages 0.038
Th1_cells 0.271
CCR 0.273
Parainflammation 0.670
APC_co_inhibition 0.703
T_cell_co−inhibition 0.790
DCs 0.797
Check−point 0.827
Tfh 0.772
APC_co_stimulation 0.581
Inflammation−promoting 0.530
TIL 0.463
aDCs 0.382
T_helper_cells 0.355
CD8+_T_cells 0.294
MHC_class_I 0.256
Type_II_IFN_Reponse 0.252
B_cells 0.223
T_cell_co−stimulation 0.184
pDCs 0.181
Type_I_IFN_Reponse 0.157
HLA 0.102
Mast_cells 0.068
Cytolytic_activity 0.062
Th2_cells 0.052
NK_cells 0.031
iDCs 0.010
−0.3 −0.2 −0.1 0.0 0.1 0.2 0.3
Correlation Coefficient
abs(cor)
0.1
0.2
0.3
0.4
0.5
pvalue
0
0.2
0.4
0.6
0.8
1

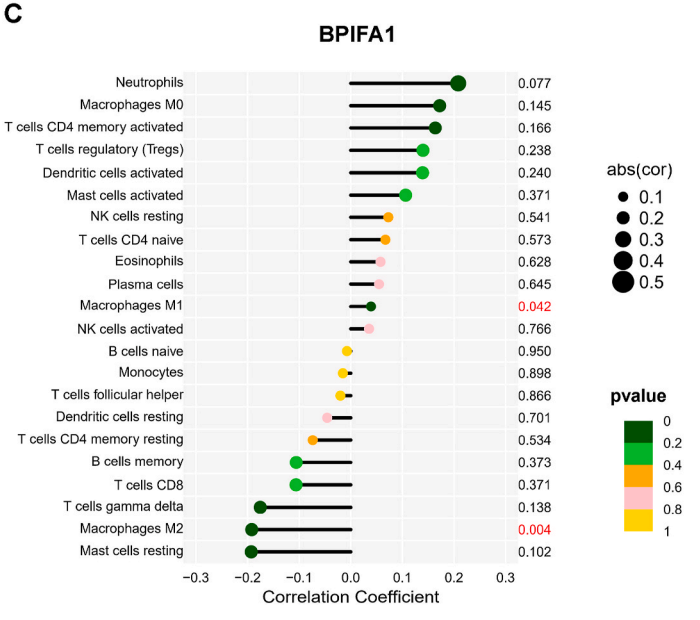
C
BPIFA1
Neutrophils 0.077
Macrophages M0 0.145
T cells CD4 memory activated 0.166
T cells regulatory (Tregs) 0.238
Dendritic cells activated 0.240
Mast cells activated 0.371
NK cells resting 0.541
T cells CD4 naive 0.573
Eosinophils 0.628
Plasma cells 0.645
Macrophages M1 0.042
NK cells activated 0.766
B cells naive 0.950
Monocytes 0.898
T cells follicular helper 0.866
Dendritic cells resting 0.701
T cells CD4 memory resting 0.534
B cells memory 0.373
T cells CD8 0.371
T cells gamma delta 0.138
Macrophages M2 0.004
Mast cells resting 0.102
−0.3 −0.2 −0.1 0.0 0.1 0.2 0.3
Correlation Coefficient
abs(cor)
0.1
0.2
0.3
0.4
0.5
pvalue
0
0.2
0.4
0.6
0.8
1

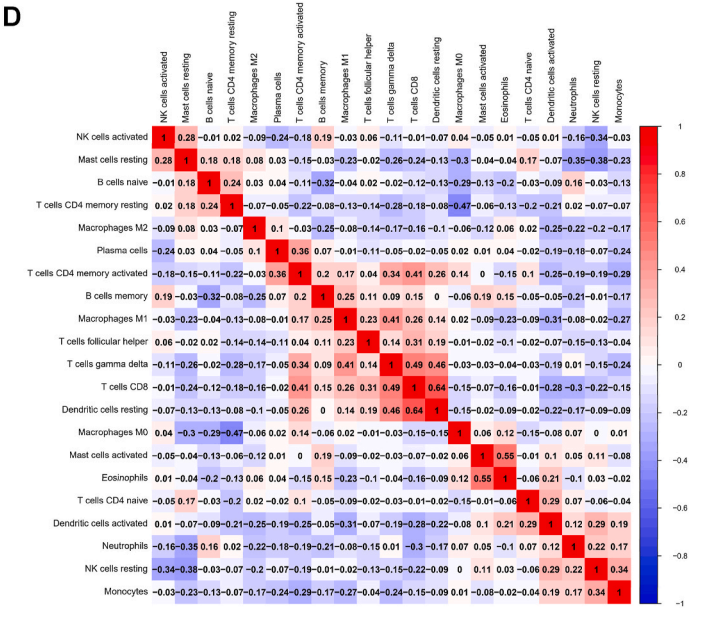
D
NK cells activated
Mast cells resting
B cells naive
T cells CD4 memory resting
Macrophages M2
Plasma cells
T cells CD4 memory activated
B cells memory
Macrophages M1
T cells follicular helper
T cells gamma delta
T cells CD8
Dendritic cells resting
Macrophages M0
Mast cells activated
Eosinophils
T cells CD4 naive
Dendritic cells activated
Neutrophils
NK cells resting
Monocytes
1
0.8
0.6
0.4
0.2
0
−0.2
−0.4
−0.6
−0.8
−1

Fig. 8. BPIFA1 correlation with macrophages in PAH tissues. (A) The MCP-counter algorithm was employed to explore the association between the BPIFA1 and the composition of immune cells, where those highlighted in red denote a statistically meaningful relationship between the gene and immune cells. (B) Utilizing the ssGSEA algorithm, the study investigated the linkage between the BPIFA1 and immune cell content, with significant correlations marked in red. (C) The CIBERSORT algorithm's application revealed the connection between BPIFA1 and immune cell abundance, with red highlights indicating statistically significant associations. (D) Correlation analysis was performed on all immune cells in the CIBERSORT algorithm. (For interpretation of the references to colour in this figure legend, the reader is referred to the Web version of this article.)

3.2. WCGNA analysis

The input matrix for conducting the WGCNA analysis comprised the expression levels of 8009 genes that exhibited a notable difference ($p < 0.05$) between normal and PAH samples. Effective sample clustering was attained, and one outlier sample was eliminated by the cutoff threshold of 50 (Fig. 3A). With the optimal soft threshold identified as 7, the relationship matrix was transformed into an adjacency matrix and subsequently into a TOM (Fig. 3B). Modules with interrelated genes were discerned based on TOM, ensuring that each module encompassed a minimum of 50 genes. Similar gene modules were consolidated, which led to the identification of four distinct modules (Fig. 3C). As shown in Fig. 3D, the magenta module had the strongest correlation ($P = -0.71$) with the presence of PAH; therefore, it was designated the core module. Additionally, the GS and MM values were computed for the 4003 genes included in the magenta module, and a scatter diagram was produced to illustrate their correlation. Interestingly, a strong correlation was observed between the GS in the core module and MM, providing additional support for our findings (Fig. 3E).

3.3. Analysis of enrichment in DEGs

The probable biological processes between the 25 differential genes and the occurrence of PAH were investigated using DO analysis to identify related diseases. The results showed that psoriatic arthritis, obesity, overnutrition, and nutritional disease may share pathogenesis with PAH, suggesting the involvement of metabolic or immune-related regulation (Fig. 4A). KEGG analysis also revealed a correlation between PAH occurrence and immunity, with the enrichment of the IL-17 signaling pathway (Fig. 4B). GO enrichment analysis further confirmed the importance of immune responses in PAH development (Fig. 4C). In addition, GSVA analysis of gene expression data from the MSigDB c7. Immunesigdb. V7.4. Symbols. GMT gene sets showed that pathways such as epithelial mesenchymal transition (EMT), interferon-γ response, mitotic spindle, and TNFA signaling via NFkb are possibly involved in the pathogenesis of PAH (Fig. 4D). Collectively, these data offer compelling evidence of the immune system's role in the development of PAH.

3.4. Predictive value of biomarkes

By merging the related genes from WGCNA, LASSO, and machine learning, a cross-referencing method was used to find the hub genes. Seven biomarkers were found as potential genes (Fig. 5A). ROC values revealed that each gene demonstrated a high degree of prognostic predictive performance. The following are the AUC values: BPIFA1 (0.775, Fig. 5B), HBA2 (0.893, Fig. 5C), HBB (0.900, Fig. 5D), LOC441081 (0.841, Fig. 5E), PI15 (0.827, Fig. 5F), S100A9 (0.847, Fig. 5G), and WIF1 (0.852, Fig. 5H).

3.5. Validation of hub biomakers

To verify the accuracy of the prognostic effect of the above 7 genes, non-coding Rnas were excluded and verified using an external validation set. Across samples of sequenced vascular endothelial tissue in the GSE15197 dataset, BPIFA1 expression was consistent (Fig. 6A), and ROC analysis exhibited good predictive performance (AUC = 0.731, Fig. 6B). In order to assess the possible utility of core biomarkers in the future for bodily fluid diagnosis, we conducted a thorough analysis of the GSE131793 whole blood sequencing sample dataset and found that BPIF1A was consistently expressed in all of the samples. Moreover, the ROC analysis showed that the AUC value of this marker was 0.740 (Fig. 6C and D). The regulatory networks of seven core genes were visualized based on the NetworkAnalyst database, including mRNA-miRNA and TF-mRNA networks (Figure S3). BPIFA1 interacts with the TFs SOX10, HOXA5, GATA2, GATA3, and SREBF1. It has a potential regulatory relationship with miRNAs, such as mir-182–5p and mir-335–5p.

3.6. Examination of variations in the immune microenvironment

To investigate the possible contribution of immunity to PAH, we performed an immune cell content analysis in different tissues using the three algorithms. The MCP-counter algorithm revealed differential expression in the monocytic lineage, T cells, neutrophils, and fibroblasts (Fig. 7A). Monocytic lineage samples had significantly higher levels in normal tissues than in PAH samples (Fig. 7B). Next, the ssGSEA algorithm was used to refine immune cell classification and identified that macrophages were differentially expressed in the monocytic lineage and were more abundant in normal tissues (Fig. 7C and D). Finally, using the CIBERSORT algorithm, we classified macrophages into three types: M0, M1, and M2 (Fig. 7E). The content of M0 type cells did not show any significant difference between the two samples (Fig. 7F). However, the PAH samples exhibited a higher proportion of M1 type cells (Fig. 7G) and a lower proportion of M2 type cells (Fig. 7H). These findings indicate that macrophages and immunological dysregulation have a role in the genesis and progression of PAH.

3.7. Correlation of BPIFA1 with macrophage in PAH

To explore the correlation between BPFA1 and immune cell content, correlation analyses were performed using three different algorithms. Using the MCP-counter algorithm, BPFA1 expression negatively correlated with the cell content of CD8 +T cells, endothelial cells, cytotoxic lymphocytes, natural killer (NK) cells, and myeloid dendritic cells (Fig. 8A). In the ssGSEA algorithm, BPFA1 expression positively correlated with macrophages but negatively correlated with NK cells and iDCs (Fig. 8B). Using the CIBERSORT algorithm, BPFA1 expression was determined to be weakly positively correlated with macrophage M1 ($r = 0.039$) and weakly negatively correlated with macrophage M2 ($r = -0.192$) (Fig. 8C). The CIBERSORT algorithm was used to conduct further correlation analysis on different immune cells. The results revealed that Macrophages M0 had a strong negative correlation ($r = -0.47$) with CD4 +T cells memory resting. Conversely, CD8 +T cells showed a significant positive correlation ($r = -0.64$) with resting dendritic cells (Fig. 8D). Therefore, we hypothesized that the core gene BPFA1 is involved in the progression of PAH by mediating macrophages M2. Detailed results of the interactions between other hub genes and immune cells are shown in Figure S4.

3.8. Validation in MCT pulmonary hypertension animal model

To validate the potential of BPIFA1 as a biomarker, we investigated its expression in a rat model of MCT-induced pH. BPIFA1 expression was markedly reduced in the MCT group compared to the normal group (Fig. 9), observed at both mRNA and protein levels. Collectively, these findings strongly indicate that BPIFA1 is a promising biomarker for pulmonary hypertension.

4. Discussion

In this investigation, a thorough analysis of the PAH was performed. Initially, 25 DEGs were identified from public datasets, and a PPI network was constructed to reveal their interactions. Subsequently, core genes were determined using 10-fold cross-validated LASSO and SVM machine learning methods, with a focus on the intersection with WGCNA. For WGCNA delineating four modules, the magenta module was highly negatively correlated to PAH occurrence, earning its designation as the core module. Enrichment analyses of the 25 DEGs highlighted associations between PAH and immune responses, metabolism, and diseases. To further refine the identification of the core genes, an integrated analysis of WGCNA, LASSO, and machine learning was performed, resulting in the

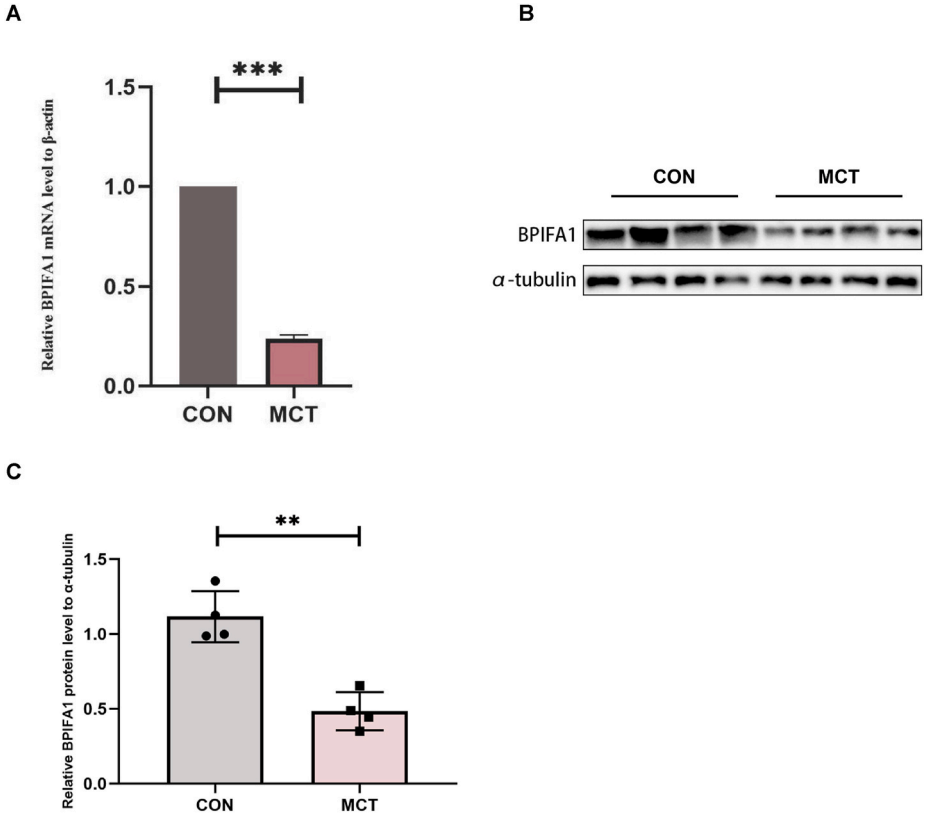

Fig. 9. Expression profile of diagnostic biomarkers in the MCT group, validated using qPCR and WB. (A) The expression level of BPIFA1 mRNA in the lungs of MCT-induced PAH subjects compared to controls. (B–C) Western blot analysis and subsequent quantification of BPIFA1 and α-tubulin in the lung tissues from subjects with MCT-induced PAH versus control subjects. *$p < 0.05$, **$p < 0.01$, and ***$p < 0.001$.

identification of seven candidate genes as potential biomarkers (BPIFA1, HBA2, HBB, LOC441081, PI15, S100A9, and WIF1). Furthermore, immune cell content analysis using the three algorithms demonstrated the differential expression of the monocytic lineage, T cells, neutrophils, and fibroblasts in patients with PAH. Notably, the CIBERSORT algorithm underscored higher M1 cell content and lower M2 cell content in PAH samples, suggesting the potential roles of macrophages and immune dysregulation in PAH development. Finally, the correlation between the core gene BPIFA1 and macrophages emphasizes its potential mediating role in PAH progression.

The enrichment analysis revealed a potential association between the IL-17 pathway and PAH. IL-17 is an inflammatory cytokine produced by T lymphocytes, playing a pivotal role in regulating immune responses [39]. Previous studies have suggested that the IL-17 pathway is important in the pathogenesis of PAH [40]. In patients with PAH, IL-17 levels are often elevated, which is potentially linked to abnormal activation of the immune system and inflammatory responses [41]. IL-17 can promote the release of inflammatory factors, triggering inflammation in the vascular wall and leading to the remodeling and narrowing of pulmonary vessels [42]. These changes may increase pulmonary arterial resistance, ultimately leading to the onset of PAH. Moreover, IL-17 may affect endothelial function and the proliferation of vascular smooth muscle cells, further affecting vascular structure and function [43]. Therefore, It is possible that activation of the IL-17 pathway is essential for the progression of PAH. GSVA analysis further enriched DEGs involving EMT, interferon-gamma response, and TNFA signaling mediated through NFκB. Pulmonary artery fibrosis has a significant phenotype [44]. Specifically, epithelial cells acquire mesenchymal characteristics through EMT, thereby enhancing cell motility and migratory capabilities [45]. Interferon-gamma, as a cytotoxic cytokine, modulates the activity of the immune system, influencing pulmonary vascular remodeling [46]. Furthermore, TNFα, functioning as a pro-inflammatory cytokine, can stimulate the production of several typical pro-inflammatory cytokines, including IL-1, IL-6, and GM-CSF, by activating the NF-κB signaling pathway. This signaling system also has a vital function in the process of pulmonary vascular remodeling [47].

Inflammation is increasingly recognized as a burgeoning area of interest, with its hallmark being the critical contribution of the immune system to immunosurveillance in the vascular environment [48]. Consequently, Increasing research has documented the substantial impact of inflammation and immunological changes in PAH [13]. In the present study, ssGSEA revealed differential expression within the monocyte lineage by using the CIBERSORT algorithm for classification. Macrophages are categorized into M0, M1, and M2 types, with higher M1 and lower M2 levels being observed in PAH. Macrophages have a crucial function in the immune system and undergo differentiation into either M1 or M2 phenotypes depending on the signals they receive from their surroundings. M1 macrophages largely contribute to inflammatory reactions and defense against pathogens, while M2 macrophages are involved in tissue healing and the resolution of inflammation [49]. In diseases such as coronary artery disease, the dynamic polarization of macrophages between M1 and M2 responds to microenvironmental stimuli within atherosclerotic plaques [50]. In addition, M2 macrophages express elevated levels of Mer receptor tyrosine kinase (MerTK), which contributes to effective phagocytosis [51]. Changes in the balance between M1/M2 macrophage phenotypes are associated with various diseases, including atherosclerosis and type 2 diabetes [52]. Studies have suggested that the M1/M2 balance is dynamic in atherosclerotic plaques, with M1 dominance during disease progression and M2 dominance during regression [52]. In diseases such as type 2 diabetes, a transition from pro-inflammatory M1 macrophages to pro-fibrotic M2 macrophages has been reported [52]. In PAH, the activity of M2 macrophages may contribute to the suppression of excessive inflammatory responses, promotion of vascular wall repair, and maintaining balance [47]. Recent studies have suggested that danazol inhibits M2 macrophage activation in rats treated with monocrotaline, effectively reducing pulmonary arterial smooth muscle cell proliferation and improving lung vascular remodeling [53]. In order to confirm the presence of alterations in macrophage polarization in patients with PAH, a study observed an imbalance in M1/M2 between MacLow-derived macrophages and monocyte-derived macrophages stimulated by doxycycline and interleukin-4 (IL-4) [54]. This finding suggests the participation of immune cells in this phenomenon, and reestablishing the equilibrium in macrophage populations may provide forthcoming therapeutic prospects, given that inflammation is a defining characteristic of PAH. Invading and inflammatory cell interaction is critical for the progression of PAH.

After the final screening, we identified seven potential biomarkers. However, only BPIFA1 demonstrated consistent stability in subsequent external datasets, a validation that was further confirmed through our MCT animal model experiments. BPIFA1, also recognized as short palate, lung, and nasal epithelium clone 1 (Splunc1), belongs to the killing/increasing permeability protein folding (Bpif) superfamily [55]. This diverse superfamily comprises proteins with a structure reminiscent of killing/increasing permeability proteins (BPI), which are known for their ability to bind lipopolysaccharide (LPS) and exhibit antimicrobial and immunoregulatory properties [56]. However, BPIFA1 expression increases in response to respiratory insults such as bacterial infections, inflammation, and cigarette smoke exposure [57]. BPIFA1 has been shown to exhibit antimicrobial activity against gram-negative and gram-positive bacteria, as well as anti-inflammatory and immunomodulatory effects [58]. Genomic and proteomic studies have indicated differential expression of Bpifa1 in lung diseases, and multifaceted BPIFA1 has been established to possess both pro-inflammatory and anti-inflammatory effects [59]. In an allergic airway inflammation model, mice lacking BPIFA1 displayed increased airway inflammation accompanied by increased eosinophil counts, augmented mucus production, airway hyperreactivity, and elevated T levels [60]. Previous research postulated that BPIFA1 does not only influence chemokine expression but also exerts a moderate chemotactic effect on macrophages and neutrophils [61]. BPIFA1 may curtail the increase in eosinophils in allergic airway inflammation models by influencing eosinophil chemotactic factors; in contrast, it may potentially contribute to an increased presence of lung neutrophils in an inhaled single-walled carbon nanotube (SWCNT) model [62]. Our results, derived from the CIBERSORT algorithm, indicate that BPIFA1 exhibits varying correlations with M1 and M2 macrophages, suggesting its potential involvement in the progression of PAH by regulating the M1/M2 macrophage ratio.

It is crucial to recognize the significant constraints of this study. The size of the sample was somewhat limited. Moreover, our results highly relied on computer analysis grounded in bioinformatics; thus, validation through in vivo and in vitro experiments is required.

We validated the differential expression of BPIFA1 at the mRNA and protein levels without experimentally confirming its specific role in PAH.

5. Conclusion

BPIFA1 is a potential diagnostic marker of PAH. Inflammation and immune dysfunction are involved in the pathogenesis of PAH, and anti-inflammatory medications have the potential to be efficacious therapies.

Ethics approval and consent to participate

All animal procedures were approved by the Experimental Animal Ethics Committee of Central South University (No. 2021SYDW0110). The authors are accountable for all aspects of this work and ensure that questions related to the accuracy or integrity of any part of the work are appropriately investigated and resolved.

Funding

This study was financially supported by the National Natural Science Foundation of China (82070055 and 82100071), and the Natural Science Foundation of Hunan Province (2024JJ6673, 2024JJ6620 and 2024JJ6692).

Data availability statement

The data associated with this study have been deposited in a publicly available repository. The repository names and accession numbers are as follows:

Repository: GEO.

Accession numbers: GSE113439, GSE117261, GSE131793, and GSE15197.

These responses provided information on the availability of the research data and contributed to transparency, which will enable other researchers to evaluate the findings and build upon the work presented in this article.

CRediT authorship contribution statement

Mukamengjiang Juaiti: Visualization, Software, Methodology, Investigation, Formal analysis, Data curation. **Yilu Feng:** Investigation, Data curation. **Yiyang Tang:** Formal analysis, Data curation. **Benhui Liang:** Data curation. **Lihuang Zha:** Methodology, Funding acquisition. **Zaixin Yu:** Writing – review & editing, Funding acquisition.

Declaration of competing interest

The authors declare that they have no known competing financial interests or personal relationships that could have appeared to influence the work reported in this paper.

Acknowledgments

Not applicable.

Appendix ASupplementary data

Supplementary data to this article can be found online at https://doi.org/10.1016/j.heliyon.2024.e29587.

References

[1] R.T. Schermuly, H.A. Ghofrani, M.R. Wilkins, F. Grimminger, Mechanisms of disease: pulmonary arterial hypertension, Nat. Rev. Cardiol. 8 (8) (2011) 443–455.
[2] N.F. Ruopp, B.A. Cockrill, Diagnosis and treatment of pulmonary arterial hypertension: a review, JAMA 327 (14) (2022) 1379–1391.
[3] J.P. Stasch, P. Pacher, O.V. Evgenov, Soluble guanylate cyclase as an emerging therapeutic target in cardiopulmonary disease, Circulation 123 (20) (2011) 2263–2273.
[4] K.W. Prins, T. Thenappan, E.K. Weir, R. Kalra, M. Pritzker, S.L. Archer, Repurposing medications for treatment of pulmonary arterial hypertension: what's old is new again, J. Am. Heart Assoc. 8 (1) (2019) e011343.
[5] G. Rådegran, B. Kjellström, B. Ekmehag, et al., Characteristics and survival of adult Swedish PAH and CTEPH patients 2000-2014, Scand. Cardiovasc. J. : SCJ 50 (4) (2016) 243–250.
[6] P.M. Hassoun, L. Mouthon, J.A. Barberà, et al., Inflammation, growth factors, and pulmonary vascular remodeling, J. Am. Coll. Cardiol. 54 (1 Suppl) (2009) S10–s19.
[7] K.R. Stenmark, M.G. Frid, B.B. Graham, R.M. Tuder, Dynamic and diverse changes in the functional properties of vascular smooth muscle cells in pulmonary hypertension, Cardiovasc. Res. 114 (4) (2018) 551–564.

[8] Y. Gao, T. Chen, J.U. Raj, Endothelial and smooth muscle cell interactions in the pathobiology of pulmonary hypertension, Am. J. Respir. Cell Mol. Biol. 54 (4) (2016) 451–460.
[9] P. Lacolley, V. Regnault, P. Segers, S. Laurent, Vascular smooth muscle cells and arterial stiffening: relevance in development, aging, and disease, Physiol. Rev. 97 (4) (2017) 1555–1617.
[10] S.A. Barman, D. Fulton, Adventitial fibroblast Nox 4 expression and ROS signaling in pulmonary arterial hypertension, Adv. Exp. Med. Biol. 967 (2017) 1–11.
[11] M.G. Frid, J.M. Thurman, K.C. Hansen, B.A. Maron, K.R. Stenmark, Inflammation, immunity, and vascular remodeling in pulmonary hypertension; Evidence for complement involvement? Global cardiology science & practice 2020 (1) (2020) e202001.
[12] M. Tomaszewski, D. Bębnowska, R. Hrynkiewicz, et al., Role of the immune system elements in pulmonary arterial hypertension, J. Clin. Med. 10 (16) (2021).
[13] A. Huertas, F. Perros, L. Tu, et al., Immune dysregulation and endothelial dysfunction in pulmonary arterial hypertension: a complex interplay, Circulation 129 (12) (2014) 1332–1340.
[14] R.R. Wang, T.Y. Yuan, J.M. Wang, et al., Immunity and inflammation in pulmonary arterial hypertension: from pathophysiology mechanisms to treatment perspective, Pharmacol. Res. 180 (2022) 106238.
[15] T. Klouda, K. Yuan, Inflammation in pulmonary arterial hypertension, Adv. Exp. Med. Biol. 1303 (2021) 351–372.
[16] R. Romero, J. Espinoza, F. Gotsch, et al., The use of high-dimensional biology (genomics, transcriptomics, proteomics, and metabolomics) to understand the preterm parturition syndrome, BJOG An Int. J. Obstet. Gynaecol. 113 (Suppl 3) (2006) 118–135. Suppl 3.
[17] V.A. de Jesus Perez, Molecular pathogenesis and current pathology of pulmonary hypertension, Heart Fail. Rev. 21 (3) (2016) 239–257.
[18] G. Sutendra, E.D. Michelakis, The metabolic basis of pulmonary arterial hypertension, Cell Metabol. 19 (4) (2014) 558–573.
[19] J.T. Leek, W.E. Johnson, H.S. Parker, A.E. Jaffe, J.D. Storey, The SVA package for removing batch effects and other unwanted variation in high-throughput experiments, Bioinformatics 28 (6) (2012) 882–883.
[20] M.E. Ritchie, B. Phipson, D. Wu, et al., Limma powers differential expression analyses for RNA-sequencing and microarray studies, Nucleic Acids Res. 43 (7) (2015) e47.
[21] D. Sjoberg, M. Curry, M. Hannum, et al., Presentation-ready Data Summary and Analytic Result Tables, 2021.
[22] K.L. Ayers, H.J. Cordell, SNP Selection in genome-wide and candidate gene studies via penalized logistic regression, Genet. Epidemiol. 34 (8) (2010) 879–891.
[23] K. Heikamp, J. Bajorath, Support vector machines for drug discovery, Expet Opin. Drug Discov. 9 (2014) 93–104.
[24] X. Zhou, D.P. Tuck, MSVM-RFE: extensions of SVM-RFE for multiclass gene selection on DNA microarray data, Bioinformatics 23 (9) (2007) 1106–1114.
[25] P. Langfelder, S. Horvath, P. Langfelder, S. Horvath, WGCNA: an R package for weighted correlation network analysis. BMC Bioinform 9: 559, BMC Bioinf. 9 (559) (2009) 559.
[26] C. von Mering, M. Huynen, D. Jaeggi, S. Schmidt, P. Bork, B. Snel, STRING: a database of predicted functional associations between proteins, Nucleic Acids Res. 31 (1) (2003) 258–261.
[27] P. Shannon, A. Markiel, O. Ozier, et al., Cytoscape: a software environment for integrated models of biomolecular interaction networks, Genome Res. 13 (11) (2003) 2498–2504.
[28] M. Ashburner, C.A. Ball, J.A. Blake, et al., Gene ontology: tool for the unification of biology. The Gene Ontology Consortium, Nat. Genet. 25 (1) (2000) 25–29.
[29] G. Yu, L.G. Wang, Y. Han, Q.Y. He, clusterProfiler: an R package for comparing biological themes among gene clusters, OMICS A J. Integr. Biol. 16 (5) (2012) 284–287.
[30] M. Kanehisa, M. Furumichi, M. Tanabe, Y. Sato, K. Morishima, KEGG: new perspectives on genomes, pathways, diseases and drugs, Nucleic Acids Res. 45 (D1) (2017) D353–d361.
[31] W.A. Kibbe, C. Arze, V. Felix, et al., Disease Ontology 2015 update: an expanded and updated database of human diseases for linking biomedical knowledge through disease data, Nucleic Acids Res. 43 (Database issue) (2015) D1071–D1078.
[32] W. Walter, F. Sánchez-Cabo, M. Ricote, GOplot: an R package for visually combining expression data with functional analysis, Bioinformatics 31 (17) (2015) 2912–2914.
[33] S. Hänzelmann, R. Castelo, J. Guinney, GSVA: gene set variation analysis for microarray and RNA-seq data, BMC Bioinf. 14 (2013) 7.
[34] A. Liberzon, A. Subramanian, R. Pinchback, H. Thorvaldsdóttir, P. Tamayo, J.P. Mesirov, Molecular signatures database (MSigDB) 3.0, Bioinformatics 27 (12) (2011) 1739–1740.
[35] T. Tomas, P. Chiara, A.E.M. Rossos, et al., mirDIP 4.1—integrative database of human microRNA target predictions, Nucleic Acids Res. (D1) (2017) D1.
[36] H. Han, J.W. Cho, S. Lee, A. Yun, I. Lee, TRRUST v2: an expanded reference database of human and mouse transcriptional regulatory interactions, Nucleic Acids Res. 46 (Database issue) (2017).
[37] M. Aaron, C. Newman Long, et al., Robust enumeration of cell subsets from tissue expression profiles, Nat. Methods 12 (2015) 453–457.
[38] E. Becht, N.A. Giraldo, L. Lacroix, B. Buttard, Estimating the population abundance of tissue-infiltrating immune and stromal cell populations using gene expression, Genome Biol. 17 (1) (2016).
[39] S. Xu, X. Cao, Interleukin-17 and its expanding biological functions, Cell. Mol. Immunol. 7 (3) (2010) 164–174.
[40] L. Wang, J. Liu, W. Wang, et al., Targeting IL-17 attenuates hypoxia-induced pulmonary hypertension through downregulation of β-catenin, Thorax 74 (6) (2019) 564–578.
[41] A. Hautefort, B. Girerd, D. Montani, et al., T-helper 17 cell polarization in pulmonary arterial hypertension, Chest 147 (6) (2015) 1610–1620.
[42] S.S. Batah, M.A. Alda, R. Rodrigues Lopes Roslindo Figueira, et al., In situ evidence of collagen V and interleukin-6/interleukin-17 activation in vascular remodeling of experimental pulmonary hypertension. Pathobiology : journal of immunopathology, Mol. Cell Biol. 87 (6) (2020) 356–366.
[43] M. Robert, P. Miossec, Effects of Interleukin 17 on the cardiovascular system, Autoimmun. Rev. 16 (9) (2017) 984–991.
[44] C.J. Ryerson, T. Hartman, B.M. Elicker, et al., Clinical features and outcomes in combined pulmonary fibrosis and emphysema in idiopathic pulmonary fibrosis, Chest 144 (1) (2013) 234–240.
[45] Y. Yun, R. Gao, H. Yue, X. Liu, G. Li, N. Sang, Polycyclic aromatic hydrocarbon (PAH)-containing soils from coal gangue stacking areas contribute to epithelial to mesenchymal transition (EMT) modulation on cancer cell metastasis, Sci. Total Environ. 580 (2017) 632–640.
[46] A.H. Sprague, R.A. Khalil, Inflammatory cytokines in vascular dysfunction and vascular disease, Biochem. Pharmacol. 78 (6) (2009) 539–552.
[47] Y. Hu, L. Chi, W.M. Kuebler, N.M. Goldenberg, Perivascular inflammation in pulmonary arterial hypertension, Cells 9 (11) (2020).
[48] M.J. Hickey, P. Kubes, Intravascular immunity: the host-pathogen encounter in blood vessels, Nat. Rev. Immunol. 9 (5) (2009) 364–375.
[49] C.D. Mills, Anatomy of a discovery: m1 and m2 macrophages, Front. Immunol. 6 (2015) 212.
[50] M. Peled, E.A. Fisher, Dynamic aspects of macrophage polarization during atherosclerosis progression and regression, Front. Immunol. 5 (2014) 579.
[51] I. Dransfield, A. Zagórska, E.D. Lew, K. Michail, G. Lemke, Mer receptor tyrosine kinase mediates both tethering and phagocytosis of apoptotic cells, Cell Death Dis. 6 (2) (2015) e1646.
[52] C. Roma-Lavisse, M. Tagzirt, C. Zawadzki, et al., M1 and M2 macrophage proteolytic and angiogenic profile analysis in atherosclerotic patients reveals a distinctive profile in type 2 diabetes, Diabetes Vasc. Dis. Res. 12 (4) (2015) 279–289.
[53] C. Tang, Y. Luo, S. Li, B. Huang, S. Xu, L. Li, Characteristics of inflammation process in monocrotaline-induced pulmonary arterial hypertension in rats, Biomedicine & pharmacotherapy = Biomedecine & pharmacotherapie 133 (2021) 111081.
[54] A. Zawia, N.D. Arnold, L. West, et al., Altered macrophage polarization induces experimental pulmonary hypertension and is observed in patients with pulmonary arterial hypertension, Arterioscler. Thromb. Vasc. Biol. 41 (1) (2021) 430–445.
[55] N. Schaefer, X. Li, M.A. Seibold, et al., The effect of BPIFA1/SPLUNC1 genetic variation on its expression and function in asthmatic airway epithelium, JCI insight 4 (8) (2019).
[56] M. Musa, K. Wilson, L. Sun, et al., Differential localisation of BPIFA1 (SPLUNC1) and BPIFB1 (LPLUNC1) in the nasal and oral cavities of mice, Cell Tissue Res. 350 (3) (2012) 455–464.
[57] Y. Liu, J.A. Bartlett, M.E. Di, et al., SPLUNC1/BPIFA1 contributes to pulmonary host defense against Klebsiella pneumoniae respiratory infection, Am. J. Pathol. 182 (5) (2013) 1519–1531.

[58] Y.A. Tsou, M.C. Tung, K.A. Alexander, et al., The role of BPIFA1 in upper airway microbial infections and correlated diseases, BioMed Res. Int. 2018 (2018) 2021890.
[59] A. Liu, B. Hefley, P. Escandon, S.E. Nicholas, D. Karamichos, Salivary exosomes in health and disease: future prospects in the eye, Int. J. Mol. Sci. 24 (7) (2023).
[60] Q. Liu, Z. Wang, W. Zhang, The multifunctional roles of short palate, lung, and nasal epithelium clone 1 in regulating airway surface liquid and participating in airway host defense, J. Interferon Cytokine Res. : the official journal of the International Society for Interferon and Cytokine Research 41 (4) (2021) 139–148.
[61] C.J. Britto, N. Niu, S. Khanal, et al., BPIFA1 regulates lung neutrophil recruitment and interferon signaling during acute inflammation, Am. J. Physiol. Lung Cell Mol. Physiol. 316 (2) (2019) L321–l333.
[62] C.J. Britto, L. Cohn, Bactericidal/Permeability-increasing protein fold-containing family member A1 in airway host protection and respiratory disease, Am. J. Respir. Cell Mol. Biol. 52 (5) (2015) 525–534.